

Dispersion of Magnetic Fields in Molecular Clouds. I

Roger H. Hildebrand^{1,2}, Larry Kirby¹, Jessie L. Dotson³, Martin Houde⁴, and John E. Vaillancourt⁵

¹*Department of Astronomy and Astrophysics and Enrico Fermi Institute, The University of Chicago, Chicago, IL 60637*

²*Department of Physics, The University of Chicago, Chicago, IL 60637*

³*NASA Ames Research Center, Moffett Field, CA 94035*

⁴*Department of Physics and Astronomy, The University of Western Ontario, London, ON, N6A 3K7, Canada*

⁵*Division of Physics, Mathematics, & Astronomy, California Institute of Technology, Pasadena, CA 91125*

Abstract

We describe a method for determining the dispersion of magnetic field vectors about large-scale fields in turbulent molecular clouds. The method is designed to avoid inaccurate estimates of magnetohydrodynamic or turbulent dispersion - and help avoiding inaccurate estimates of field strengths - due to large-scale, non-turbulent field structure when using the well-known method of Chandrasekhar and Fermi. Our method also provides accurate, independent estimates of the turbulent to large-scale magnetic field strength ratio. We discuss applications to the molecular clouds OMC-1, M17, and DR21(Main).

Subject headings: ISM: clouds — ISM: magnetic fields — polarization — turbulence

1. Introduction

Chandrasekhar & Fermi (1953) used the dispersion of starlight polarization vectors about contours of Galactic latitude (Hiltner 1949) — together with estimates of gas density and line-of-sight velocity dispersion — to determine the strength of the magnetic field in the arms of the Galaxy. The same technique, “The Chandrasekhar-Fermi, ‘CF’, method”, has been applied, with modifications, to estimates of field strengths in the relatively dense medium of molecular clouds at varying temperature, wavelengths, sensitivities, and resolutions (e.g., Lai et al. 2001, 2002, 2003; Crutcher et al. 2004; Houde 2004; Girart et al. 2006; Curran & Chrysostomou 2007).

The basis for deriving field strengths from dispersion measurements is the same for observations of Galactic arms or molecular clouds: in either case dispersion decreases as the field strengthens.

But in the case of the Galactic arms, the dispersion is due to magnetohydrodynamic (MHD) waves; the displacements are perpendicular to the direction of propagation. In the case of turbulent dispersion in molecular clouds, there is no preferred direction. The turbulent component can be in any orientation.

Moreover, in dense clouds, the field may have structure due to effects such as differential rotation, gravitational collapse, or expanding H II regions; i.e., structure not accounted for by the basic CF analysis. Consequently, dispersion measured about mean fields, assumed straight, may be much larger than should be attributed to MHD waves or turbulence. Dispersion measured about model large-scale fields (Schleuning 1998; Lai et al. 2002; Girart et al. 2006) that give approximate fits to a polarization map will result in better estimates but still give inaccurate values of the turbulent component, since they are unlikely to perfectly match the true morphology of the large-scale magnetic field. In this paper we describe a method for determining magnetic field dispersion about local structured fields, without assuming any model for the large-scale field. This method also provides accurate, independent estimates of the turbulent to large-scale magnetic field strength ratio.

We begin (§2) by discussing difficulties one must overcome in order to infer turbulent structure from polarization maps, regardless of large-scale effects. In §3, we present the method and in §4, we give applications to the molecular clouds OMC-1, M17, and DR21(Main). Detailed derivations resulting in the relations and functions used in the aforementioned sections, as well as the data analysis, will be found in the appendices at the end of the paper.

2. Difficulties in Deriving the Turbulent Structure from Polarized Emission

Turbulent velocities of gas motion within and between clumps of material along the line of sight can often be inferred from the widths and centers of molecular lines (e.g., Kleiner & Dickman 1984, 1985, 1987). But dust polarization measurements of dispersion in magnetic field direction do not separate contributions from either volume elements located along the line of sight or across the area subtended by the telescope beam. Hence the measured angular dispersion tends to be a smoothed version of the true dispersion (Myers & Goodman 1991; Wiebe & Watson 2004). Nonetheless, a corresponding average of the dispersion remains and is measurable; for a given object observations will thus reveal a higher degree of dispersions when they are realized at an accordingly higher spatial resolution.

A potentially fruitful line of attack for estimating magnetic field strengths relies on comparisons of observed and simulated maps of the net polarization (e.g., Ostriker et al. 2001; Heitsch et al. 2001; Falceta-Gonçalves et al. 2008). If the simulations are computed for the resolution, column density, and other characteristics of the cloud under study, and if they are computed for several models of the key variables (e.g., field strength and turbulent fraction), then one can find the model giving the best fit to the observations. A valid simulation must also take into account temperatures (Vaillancourt

2002) and grain alignment efficiencies in different environments (Hoang & Lazarian 2008). The comparisons are facilitated if both the observations and the simulations are presented in tables of Stokes parameters, so that each can be analyzed in the same way. The various modifications of the CF method that have been used to relate net dispersion to field strength (e.g., Ostriker et al. 2001; Padoan et al. 2001; Heitsch et al. 2001; Kudoh & Basu 2003; Houde 2004) are, in effect, first-order substitutes for simulations.

But a meaningful comparison between simulations and observations can only be achieved if a reliable estimate of the spatially averaged angular dispersion can be secured experimentally. It would therefore be advantageous if a more general method, which does not depend on any assumption concerning the morphology of the large-scale magnetic field, were devised. The method we describe in the following section allows for the evaluation of the plane-of-the-sky turbulent angular dispersion in molecular clouds while avoiding inaccurate estimates of the turbulence and corresponding inaccurate estimates of field strengths due to distortions in polarization position angles by large-scale non-turbulent effects. This method can lead to valid estimates of magnetic field strengths only under conditions such that the Chandrasekhar-Fermi method can be properly applied: a smooth, low noise, polarization map, precise measured densities and gas velocities that are moderately uniform, and an adequate accounting of the integration process implicit to polarization measurements. This latter aspect will be addressed in a subsequent paper.

3. A Function to Describe Dispersion about Large-scale Fields

Consider a map precisely showing the angle $\Phi(\mathbf{x})$ of the (two-dimensional) plane-of-the-sky projected magnetic field vector $\mathbf{B}(\mathbf{x})$ at many points in a molecular cloud. We obtain a measure of the difference in angle, $\Delta\Phi(\ell) \equiv \Phi(\mathbf{x}) - \Phi(\mathbf{x} + \ell)$, between the $N(\ell)$ pairs of vectors separated by displacements ℓ , also restricted to the plane-of-the-sky, through the following function

$$\langle \Delta\Phi^2(\ell) \rangle^{1/2} \equiv \left\{ \frac{1}{N(\ell)} \sum_{i=1}^{N(\ell)} [\Phi(\mathbf{x}) - \Phi(\mathbf{x} + \ell)]^2 \right\}^{1/2}, \quad (1)$$

where $\langle \dots \rangle$ denotes an average and $\ell = |\ell|$. The square of equation (1) is also often referred to as a “structure function” (of the second order in this case; see Falceta-Gonçalves et al. 2008; Frisch 1995), but for our applications we shall refer to it as the “dispersion function” and assume that it is isotropic (i.e., it only depends on the magnitude of the displacement, ℓ , and not its orientation). We seek to determine how this quantity varies as a function of ℓ .

To do so, we will assume that the magnetic field $\mathbf{B}(\mathbf{x})$ is composed of a large-scale, structured field, $\mathbf{B}_0(\mathbf{x})$, and a turbulent (or random) component, $\mathbf{B}_t(\mathbf{x})$, which are statistically independent. We also limit ourselves to cases where $\delta < \ell \ll d$, where δ is the correlation length characterizing $\mathbf{B}_t(\mathbf{x})$ and d is the typical length scale for variations in $\mathbf{B}_0(\mathbf{x})$.

Focusing on $\mathbf{B}_0(\mathbf{x})$ we would expect its contribution to the dispersion function to increase (since $\langle \Delta\Phi^2(\ell) \rangle$ is positive definite) almost linearly starting at $\ell = 0$ and for small displacements $\ell \ll d$, as would be expected from the Taylor expansion of any smoothly varying quantity. We denote by m the slope characterizing this linear behavior. We also expect a contribution from the turbulent component of the magnetic field $\mathbf{B}_t(\mathbf{x})$. This contribution will vary from zero as $\ell \rightarrow 0$ (when the two magnetic field vectors are co-aligned) to a maximum average value when the displacement exceeds the correlation length δ characterizing $\mathbf{B}_t(\mathbf{x})$. More precisely, we expect that the turbulent contribution to the angular dispersion will be a constant, which we denote by b , as long as $\ell > \delta$. These two contributions must be combined quadratically, since the large-scale and turbulent fields are statistically independent, to yield

$$\langle \Delta\Phi^2(\ell) \rangle \simeq b^2 + m^2\ell^2 \quad (2)$$

when $\delta < \ell \ll d$.

A more formal and rigorous derivation of equation (2) is established in Appendix A under the further assumptions of homogeneity and isotropy in the magnetic field strength over space. Although these assumptions are unlikely to be realized across molecular clouds, this level of idealization is necessary to allow us to gain insights on, and some quantitative measure of, the importance of the turbulent component of the magnetic field in molecular clouds.

In reality, the measured dispersion function from a polarization map will also include a contribution, $\sigma_M(\ell)$, due to measurement uncertainties on the polarization angles $\Phi(\mathbf{x})$ that must be added (quadratically) to equation (2). The square of the total measured dispersion function then becomes

$$\langle \Delta\Phi^2(\ell) \rangle_{\text{tot}} \simeq b^2 + m^2\ell^2 + \sigma_M^2(\ell). \quad (3)$$

when $\delta < \ell \ll d$. The function $\langle \Delta\Phi^2(\ell) \rangle_{\text{tot}}$, not $\langle \Delta\Phi^2(\ell) \rangle$, is the one calculated from a polarization map (from an averaging process similar to equation [1]), and will thus contain separate components due to the large-scale structure (i.e., $m\ell$), the turbulent dispersion about the large-scale field (i.e., b , the quantity we wish to measure), and measurement uncertainties (i.e., $\sigma_M(\ell)$).

If there were no turbulence and no measurement uncertainties, then, for $\ell \ll d$ the measured dispersion function would be a straight line with zero intercept, $\langle \Delta\Phi(\ell)^2 \rangle_{\text{tot}}^{1/2} = m\ell$ (see Figure 1, Curve A). Taking the measurement uncertainty, $\sigma_M(\ell)$, into account, the line would be displaced upward as specified by equation (3) (Curve B, where σ_M was assumed to be independent of ℓ). Likewise when we next consider turbulence, the curve will again be displaced upward in the same manner (Curve C) except at values of ℓ below the angular resolution scale at which the observations were made (Curve D), or below the turbulent correlation scale δ (Curve E). Theoretical and observational estimates of δ for molecular clouds are on the order of 1 mpc (Lazarian et al. 2004;

Li & Houde 2008, respectively), well below the size of the telescope beam with which the observations presented in this paper were obtained. Although it has not yet been feasible to resolve δ , it is now feasible to determine the turbulent dispersion at scales comparable to the approximately linear portion of $\langle \Delta \Phi(\ell)^2 \rangle_{\text{tot}}^{1/2}$.

Notice that $\sigma_{\text{M}}(\ell)$ can be accurately determined through the uncertainties on the measured polarization angles of each pair of points used in the calculation of $\langle \Delta \Phi(\ell)^2 \rangle_{\text{tot}}$, and by then subtracting its square to obtain $\langle \Delta \Phi(\ell)^2 \rangle$. As the number and precision of the vectors improve, equation (2) can be fitted to the data for $\delta < \ell \ll d$, and the intercept at $\ell = 0$ provides us with the turbulent contribution, b^2 , to the square of the angular dispersion.

The Chandrasekhar-Fermi method for evaluating strength of the plane-of-the-sky component of the large-scale magnetic field (Chandrasekhar & Fermi 1953) implies that

$$\frac{\delta B}{B_0} \simeq \frac{\sigma(v)}{V_A}, \quad (4)$$

where δB stands for the variation in the magnetic field about the large-scale field B_0 , $\sigma(v)$ is the one-dimensional velocity dispersion of the gas (of mass density ρ) coupled to the magnetic field, and

$$V_A = \frac{B_0}{\sqrt{4\pi\rho}} \quad (5)$$

is the Alfvén speed. It is further assumed that the dispersion, σ_{Φ} , in the polarization angles $\Phi(\mathbf{x})$ across a map is given by

$$\sigma_{\Phi} \simeq \frac{\delta B}{B_0}. \quad (6)$$

The combination of equations (4), (5), and (6) allows for the aforementioned determination of the plane-of-the-sky component of the large-scale magnetic field strength as a function of ρ , $\sigma(v)$ (determined from the width of appropriate spectral line profiles), and σ_{Φ} (determined from polarization measurements).

It is shown with equation (A24) in Appendix A that the ratio of the turbulent to large-scale magnetic field strength is given by

$$\frac{\langle B_{\text{t}}^2 \rangle^{1/2}}{B_0} = \frac{b}{\sqrt{2 - b^2}}. \quad (7)$$

It is therefore apparent that we should make the correspondence $\langle B_{\text{t}}^2 \rangle^{1/2} \rightarrow \delta B$ and that

$$\begin{aligned}
B_0 &\simeq \sqrt{(2 - b^2) 4\pi\rho} \frac{\sigma(v)}{b} \\
&\simeq \sqrt{8\pi\rho} \frac{\sigma(v)}{b},
\end{aligned} \tag{8}$$

where the last equation applies when $B_t \ll B_0$. The fact that the turbulent dispersion, b , is to be divided by approximately $\sqrt{2}$ before being inserted the Chandrasekhar-Fermi equation is readily understood by the fact that (neglecting the contribution of the large-scale field)

$$\begin{aligned}
\langle \Delta\Phi^2(\ell) \rangle &= \langle [\Phi(\mathbf{x}) - \Phi(\mathbf{x} + \ell)]^2 \rangle \\
&= 2 \left(\langle \Phi^2 \rangle - \langle \Phi \rangle^2 \right) \\
&= 2\sigma_\Phi^2,
\end{aligned}$$

when $\ell > \delta$. Since we also know that $\langle \Delta\Phi^2(\ell) \rangle = b^2$ at these scales, we then find that $b^2 = 2\sigma_\Phi^2$, which is consistent with equations (6) and (7).

It should be noted that the combination of equations (7) and (8) allows, in principle, for the determination of both the large-scale and turbulent magnetic fields' strength from polarization and spectroscopy data.

4. Applications to the Molecular Clouds OMC-1, M17, and DR21(Main)

Using data from the polarimeter Hertz (Dowell et al. 1998) at the Caltech Submillimeter Observatory at 350 μm , we have measured dispersion functions for the molecular clouds OMC-1, M17, and DR21(Main). These data are discussed in detail in Houde et al. (2004) for OMC-1, Houde et al. (2002) for M17, and Kirby (2009) for DR21(Main). Figure 2 shows the results for all sources. More details on the data analysis will be found in Appendix B.

For each object, we show $\langle \Delta\Phi^2(\ell) \rangle^{1/2}$ over the cloud along with the best fit from equation (2) using the first three data points to ensure that $\ell \ll d$, as much as possible. The measurement uncertainties were removed prior to operating the fits to the corresponding data sets. The turbulent contribution to the total angular dispersion is determined by the zero intercept of the fit to the data at $\ell = 0$. The net turbulent component, b , is 0.18 ± 0.01 rad (10.4 ± 0.6 deg), 0.12 ± 0.02 rad (6.8 ± 1.3 deg), and 0.15 ± 0.01 rad (8.3 ± 0.3 deg) for M17, DR21(Main), and OMC-1, respectively.

Although large variations in density within the observed regions prevent a reliable estimate in the field strength at precise locations, it is still possible to give some average value for the large-scale and turbulent field strengths. To do so we use representative line width measurements from H^{13}CO^+

$J = 3 \rightarrow 2$ detections within the three clouds. For OMC-1 and M17 we have used the corresponding measurements published in Houde et al. (2000) (more precisely, an average of the variances obtained at the two positions listed for M17), while for DR21(Main) we have used previously unpublished data. This molecular species is well suited for this as the effective density needed for line detection with the aforementioned transition ($n_{\text{eff}} \sim 10^5 \text{ cm}^{-3}$, see Evans 1999) is close to the densities at which dust continuum emission is detected at the measured wavelength. Also, the corresponding spectral lines are likely to be optically thin (like the dust continuum) and an ion molecule such as this one is better coupled to the magnetic field (and the dust) than corresponding neutral species (e.g., H^{13}CN for the same rotational transition) over the whole turbulent energy density spectrum (Li & Houde 2008). Therefore, using a density of 10^5 cm^{-3} and a mean molecular weight of 2.3 we obtain the results shown in Table 1. As a simple comparison, the values of dispersion shown in the table are approximately three times lower than would be obtained if one naively calculated the dispersions about the global mean field (i.e., the field direction defined by the mean of all polarization vectors in the corresponding map). More precisely, we get dispersions of 27.2, 21.0, and 26.8 degrees about the global mean field orientation for M17, DR21(Main), and OMC-1, respectively.

We wish to emphasize the fact that the quoted values for B_0 could not be precise to better than a factor of a few due to a lack of precise gas density numbers. Moreover, the values for the large-scale magnetic field strength we derived are up to an order of magnitude higher than those obtained with other observational means (cf., the results of Crutcher et al. (1999) for OMC-1 and M17 using CN Zeeman measurements). These high values are in part the result of the smaller angular dispersions obtained using our technique as compared to more common methods used when applying the Chandrasekhar-Fermi equation (e.g., model fits to large-scale fields). One must keep in mind, however, that the process of signal integration through the thickness of the cloud and across the telescope beam that is inherent to polarization measurements has not been taken into account. We will show in a subsequent publication how this situation is rectified when these considerations (and others) are carefully taken into account (Myers & Goodman 1991; Ostriker et al. 2001; Wiebe & Watson 2004). Nevertheless, the turbulent to large-scale magnetic field strength ratio is precisely evaluated through our equation (7).

5. Summary

We have described a method to estimate plane-of-the-sky turbulent dispersion in molecular clouds while avoiding inaccurate estimates of the turbulence and corresponding inaccurate estimates of field strengths due to distortions in polarization position angles by large-scale non-turbulent effects. The method does not depend on any model of the large-scale field. We plot a “dispersion function”, the mean absolute difference in angle between pairs of vectors as a function of their displacement ℓ and show that this function increases approximately linearly for displacements greater than the instrument resolution, greater than the correlation length, δ , and less than the typical length scale, d , for variations in the large-scale magnetic field (§4). We emphasize that this

method can lead to valid estimates of magnetic field strengths only under conditions such that the Chandrasekhar-Fermi method can be properly applied: a smooth, low noise, polarization map, precise measured densities and gas velocities that are moderately uniform, and an adequate accounting of the integration process implicit to polarization measurements. This method, however, provides accurate estimates of the turbulent to large-scale magnetic field strength ratio.

Although the resolution of the instruments now available are not adequate to directly determine the correlation length, δ , one can still determine the dispersion in the fields at scales where $\delta < \ell \ll d$ for the angular dispersion function. We have successfully done this for the OMC-1, M17, and DR21(Main) molecular clouds.

We thank Shantanu Basu for helpful discussions. This work has been supported in part by NSF grants AST 05-05230, AST 02-41356, and AST 05-05124. L.K. acknowledges support from the Department of Astronomy and Astrophysics of the University of Chicago. M.H.’s research is funded through the NSERC Discovery Grant, Canada Research Chair, Canada Foundation for Innovation, Ontario Innovation Trust, and Western’s Academic Development Fund programs. J.E.V. acknowledges support from the CSO, which is funded through NSF AST 05-40882.

A. Dispersion Relation Derivation

A.1. Analysis in Three Dimensions

Let us define the total magnetic field $\mathbf{B}(\mathbf{x})$ as being composed of a deterministic, $\mathbf{B}_0(\mathbf{x})$, and a turbulent (or random), $\mathbf{B}_t(\mathbf{x})$, components such that

$$\mathbf{B}(\mathbf{x}) = \mathbf{B}_0(\mathbf{x}) + \mathbf{B}_t(\mathbf{x}). \quad (\text{A1})$$

These quantities have the following averages at points \mathbf{x} and \mathbf{y}

$$\begin{aligned} \langle \mathbf{B}_0(\mathbf{x}) \rangle &= \mathbf{B}_0(\mathbf{x}) \\ \langle \mathbf{B}_0(\mathbf{x}) \cdot \mathbf{B}_0(\mathbf{y}) \rangle &= \mathbf{B}_0(\mathbf{x}) \cdot \mathbf{B}_0(\mathbf{y}) \\ \langle \mathbf{B}_t(\mathbf{x}) \rangle &= 0 \\ \langle \mathbf{B}_0(\mathbf{x}) \cdot \mathbf{B}_t(\mathbf{y}) \rangle &= \langle \mathbf{B}_0(\mathbf{x}) \rangle \cdot \langle \mathbf{B}_t(\mathbf{y}) \rangle = 0. \end{aligned} \quad (\text{A2})$$

We will further assume homogeneity in the field strength over space. That is,

$$\begin{aligned} \langle \mathbf{B}_0^2(\mathbf{x}) \rangle &= \langle \mathbf{B}_0^2(\mathbf{y}) \rangle = B_0^2 \\ \langle \mathbf{B}_t^2(\mathbf{x}) \rangle &= \langle \mathbf{B}_t^2(\mathbf{y}) \rangle = \langle \mathbf{B}_t^2 \rangle. \end{aligned} \quad (\text{A3})$$

Let us now consider the quantity

$$\langle \cos [\Delta \Phi_{3D}(\ell)] \rangle \equiv \frac{\langle \mathbf{B}(\mathbf{x}) \cdot \mathbf{B}(\mathbf{x} + \ell) \rangle}{[\langle B^2(\mathbf{x}) \rangle \langle B^2(\mathbf{x} + \ell) \rangle]^{1/2}}. \quad (\text{A4})$$

The quantity $\Delta \Phi_{3D}(\ell)$ is the angle difference between two magnetic field (or polarization) vectors separated by a distance ℓ , the average of its square is the function that we wish to evaluate through polarization measurements (albeit in two dimensions, see §A.2). Using equations (A1) and (A2) we find that the numerator of equation (A4) (i.e., the autocorrelation of the total magnetic field; see Frisch 1995) becomes

$$\langle \mathbf{B}(\mathbf{x}) \cdot \mathbf{B}(\mathbf{x} + \ell) \rangle = B_0^2 + \left\langle \mathbf{B}_0(\mathbf{x}) \cdot \left[\sum_{n=1}^{\infty} \frac{\ell^n}{n!} (\mathbf{e}_\ell \cdot \nabla)^n \mathbf{B}_0(\mathbf{x}) \right] \right\rangle + \langle \mathbf{B}_t(\mathbf{x}) \cdot \mathbf{B}_t(\mathbf{x} + \ell) \rangle, \quad (\text{A5})$$

where we used the Taylor expansion

$$\mathbf{B}_0(\mathbf{x} + \ell) = \mathbf{B}_0(\mathbf{x}) + \sum_{n=1}^{\infty} \frac{\ell^n}{n!} (\mathbf{e}_\ell \cdot \nabla)^n \mathbf{B}_0(\mathbf{x}), \quad (\text{A6})$$

with \mathbf{e}_ℓ the unit vector in the direction of ℓ .

If we introduce d the scale length characterizing (large-scale) variations in \mathbf{B}_0 and we consider situations where $\ell = |\ell| \ll d$, then we would expect that only the first term in the summation on the right hand side of equation (A6) would need to be retained. If we define φ_i as the angle between the gradient of the i -component (i.e., $i = x, y, z$) of \mathbf{B}_0 and \mathbf{e}_ℓ , then when averaging over a large polarization map we have

$$\langle B_{0,i}(\mathbf{x}) [\ell (\mathbf{e}_\ell \cdot \nabla) B_{0,i}(\mathbf{x})] \rangle = \ell B_{0,i}(\mathbf{x}) |\nabla B_{0,i}| \langle \cos(\varphi_i) \rangle. \quad (\text{A7})$$

But since \mathbf{e}_ℓ is equally likely to be oriented in any direction over the whole map we have $\langle \cos(\varphi_i) \rangle = 0$ and the first order term of the Taylor expansion (i.e., equation [A7]) cancels out. It therefore follows that the first non-vanishing term in the summation on the right hand side of equation (A6) is of second order with

$$\left\langle \mathbf{B}_0(\mathbf{x}) \cdot \left[\sum_{n=1}^{\infty} \frac{1}{n!} (\ell \cdot \nabla)^n \mathbf{B}_0(\mathbf{x}) \right] \right\rangle \simeq \frac{1}{2} \left\langle \mathbf{B}_0(\mathbf{x}) \cdot (\mathbf{e}_\ell \cdot \nabla)^2 \mathbf{B}_0(\mathbf{x}) \right\rangle \ell^2. \quad (\text{A8})$$

when $\ell \ll d$. If we also assume stationarity for the turbulent magnetic field, then we define the autocorrelation of the turbulent field as

$$\langle \mathbf{B}_t \cdot \mathbf{B}_t(\ell) \rangle \equiv \langle \mathbf{B}_t(\mathbf{x}) \cdot \mathbf{B}_t(\mathbf{x} + \ell) \rangle, \quad (\text{A9})$$

which, if we now define δ as the correlation length for $\mathbf{B}_t(\mathbf{x})$, has the following limits

$$\langle \mathbf{B}_t \cdot \mathbf{B}_t(\ell) \rangle = \begin{cases} \langle B_t^2 \rangle, & \text{when } \ell \rightarrow 0 \\ 0, & \text{when } \ell > \delta \end{cases} \quad (\text{A10})$$

since the turbulent field is assumed uncorrelated over separations exceeding δ and $\langle \mathbf{B}_t \rangle = 0$ from the third of equations (A2). Inserting equations (A8) and (A9) into equation (A5) we have

$$\langle \mathbf{B}(\mathbf{x}) \cdot \mathbf{B}(\mathbf{x} + \ell) \rangle \simeq B_0^2(\mathbf{x}) + \frac{1}{2} \left\langle \mathbf{B}_0(\mathbf{x}) \cdot (\mathbf{e}_\ell \cdot \nabla)^2 \mathbf{B}_0(\mathbf{x}) \right\rangle \ell^2 + \langle \mathbf{B}_t \cdot \mathbf{B}_t(\ell) \rangle, \quad (\text{A11})$$

when $\ell \ll d$.

Using the assumed homogeneity in the fields' strength (i.e., equations [A3]) the denominator of equation (A4) can be readily simplified to

$$\begin{aligned} [\langle B^2(\mathbf{x}) \rangle \langle B^2(\mathbf{x} + \ell) \rangle]^{1/2} &= \langle B^2 \rangle \\ &= \langle B_0^2 + B_t^2 + 2 \langle \mathbf{B}_0 \cdot \mathbf{B}_t \rangle \rangle, \end{aligned}$$

which, with the fourth of equations (A2), becomes

$$[\langle B^2(\mathbf{x}) \rangle \langle B^2(\mathbf{x} + \ell) \rangle]^{1/2} = B_0^2 + \langle B_t^2 \rangle. \quad (\text{A12})$$

If we further assume isotropy over space (i.e., $\Delta\Phi_{3D}(\ell) = \Delta\Phi_{3D}(\ell)$) and insert equations (A11) and (A12) into equation (A4) we have

$$\langle \cos[\Delta\Phi_{3D}(\ell)] \rangle \simeq 1 - \frac{\langle B_t^2 \rangle - \langle \mathbf{B}_t \cdot \mathbf{B}_t(\ell) \rangle - \frac{1}{2} \left\langle \mathbf{B}_0(\mathbf{x}) \cdot (\mathbf{e}_\ell \cdot \nabla)^2 \mathbf{B}_0(\mathbf{x}) \right\rangle \ell^2}{B_0^2 + \langle B_t^2 \rangle}, \quad (\text{A13})$$

when $\ell \ll d$. For cases where $\Delta\Phi_{3D}(\ell)$ is small equation (A13) simplifies to

$$\langle \Delta\Phi_{3D}^2(\ell) \rangle \simeq \frac{2[\langle B_t^2 \rangle - \langle \mathbf{B}_t \cdot \mathbf{B}_t(\ell) \rangle]}{B_0^2 + \langle B_t^2 \rangle} - \frac{\left\langle \mathbf{B}_0(\mathbf{x}) \cdot (\mathbf{e}_\ell \cdot \nabla)^2 \mathbf{B}_0(\mathbf{x}) \right\rangle}{B_0^2 + \langle B_t^2 \rangle} \ell^2, \quad (\text{A14})$$

still when $\ell \ll d$.

Examining equation (A10) we recover the behavior of the turbulent contribution to $\langle \Delta \Phi_{3D}^2(\ell) \rangle$ (i.e., the first term on the right-hand side of equation [A14]) described in §3 that goes from 0 when $\ell \rightarrow 0$ to a constant, which we now define as b_{3D}^2 , when $\ell > \delta$. The data sets analyzed in this paper are such that $\ell > \delta$ in all cases. We therefore find that the dispersion function is of the form

$$\langle \Delta \Phi_{3D}^2(\ell) \rangle \simeq b_{3D}^2 + m_{3D}^2 \ell^2, \quad (\text{A15})$$

with

$$b_{3D}^2 = \frac{2 \langle B_t^2 \rangle}{B_0^2 + \langle B_t^2 \rangle}$$

when $\delta < \ell \ll d$. Once again, we identify b_{3D} with the constant contribution stemming from the turbulent field to the total angular dispersion, while the larger scale contribution due to variations in the large-scale field \mathbf{B}_0 is accounted for by the presence of a term proportional to ℓ^2 in equation (A15).

A.2. Analysis in Two Dimensions

The analysis presented above can still be used when we limit ourselves to two dimensions. This is needed in order to enable comparisons with polarization measurements, which only probe the plane-of-the-sky component, \mathbf{B}_\parallel , of the magnetic field. Defining \mathbf{e}_\perp as the unit vector directed along the line-of-sight we have for the total magnetic field

$$\mathbf{B}_\parallel = \mathbf{B} - (\mathbf{B} \cdot \mathbf{e}_\perp) \mathbf{e}_\perp, \quad (\text{A16})$$

and similar relations for \mathbf{B}_0 and \mathbf{B}_t .

We need to evaluate, among others, the following autocorrelation

$$\langle \mathbf{B}_\parallel(\mathbf{x}) \cdot \mathbf{B}_\parallel(\mathbf{x} + \boldsymbol{\ell}) \rangle = \langle \mathbf{B}(\mathbf{x}) \cdot \mathbf{B}(\mathbf{x} + \boldsymbol{\ell}) \rangle - \langle [\mathbf{B}(\mathbf{x}) \cdot \mathbf{e}_\perp] [\mathbf{B}(\mathbf{x} + \boldsymbol{\ell}) \cdot \mathbf{e}_\perp] \rangle, \quad (\text{A17})$$

where the separation $\boldsymbol{\ell}$ is now limited to the plane-of-the-sky. The last term on the right hand-side can be transformed to

$$\begin{aligned} \langle [\mathbf{B}(\mathbf{x}) \cdot \mathbf{e}_\perp] [\mathbf{B}(\mathbf{x} + \boldsymbol{\ell}) \cdot \mathbf{e}_\perp] \rangle &= \langle \{ [\mathbf{B}_0(\mathbf{x}) + \mathbf{B}_t(\mathbf{x})] \cdot \mathbf{e}_\perp \} \{ [\mathbf{B}_0(\mathbf{x} + \boldsymbol{\ell}) + \mathbf{B}_t(\mathbf{x} + \boldsymbol{\ell})] \cdot \mathbf{e}_\perp \} \rangle \\ &= B_{0,\perp}^2 + \langle [\mathbf{B}_t(\mathbf{x}) \cdot \mathbf{e}_\perp] [\mathbf{B}_t(\mathbf{x} + \boldsymbol{\ell}) \cdot \mathbf{e}_\perp] \rangle. \end{aligned} \quad (\text{A18})$$

Using the same method that led to equation (A12) in the three-dimensional case we also have that

$$\left[\left\langle B_{\parallel}^2(\mathbf{x}) \right\rangle \left\langle B_{\parallel}^2(\mathbf{x} + \boldsymbol{\ell}) \right\rangle \right]^{1/2} = B_{0,\parallel}^2 + \left\langle B_{t,\parallel}^2 \right\rangle. \quad (\text{A19})$$

We now introduce the function

$$\langle \cos [\Delta \Phi(\boldsymbol{\ell})] \rangle \equiv \frac{\langle \mathbf{B}_{\parallel}(\mathbf{x}) \cdot \mathbf{B}_{\parallel}(\mathbf{x} + \boldsymbol{\ell}) \rangle}{\left[\left\langle B_{\parallel}^2(\mathbf{x}) \right\rangle \left\langle B_{\parallel}^2(\mathbf{x} + \boldsymbol{\ell}) \right\rangle \right]^{1/2}}, \quad (\text{A20})$$

which upon inserting equations (A11), (A17), (A18), and (A19) with the condition of space isotropy becomes

$$\langle \cos [\Delta \Phi(\boldsymbol{\ell})] \rangle \simeq 1 - \frac{\left\langle B_{t,\parallel}^2 \right\rangle - \langle \mathbf{B}_{t,\parallel} \cdot \mathbf{B}_{t,\parallel}(\boldsymbol{\ell}) \rangle - \frac{1}{2} \left\langle \mathbf{B}_0(\mathbf{x}) \cdot (\mathbf{e}_{\ell} \cdot \nabla)^2 \mathbf{B}_0(\mathbf{x}) \right\rangle \ell^2}{B_{0,\parallel}^2 + \left\langle B_{t,\parallel}^2 \right\rangle},$$

when $\ell \ll d$ and where

$$\langle \mathbf{B}_{t,\parallel} \cdot \mathbf{B}_{t,\parallel}(\boldsymbol{\ell}) \rangle = \langle \mathbf{B}_t \cdot \mathbf{B}_t(\boldsymbol{\ell}) \rangle - \langle [\mathbf{B}_t(\mathbf{x}) \cdot \mathbf{e}_{\perp}] [\mathbf{B}_t(\mathbf{x} + \boldsymbol{\ell}) \cdot \mathbf{e}_{\perp}] \rangle.$$

If we further consider $\Delta \Phi(\boldsymbol{\ell})$ to be small, then we find

$$\langle \Delta \Phi^2(\boldsymbol{\ell}) \rangle \simeq \frac{2 \left[\left\langle B_{t,\parallel}^2 \right\rangle - \langle \mathbf{B}_{t,\parallel} \cdot \mathbf{B}_{t,\parallel}(\boldsymbol{\ell}) \rangle \right]}{B_{0,\parallel}^2 + \left\langle B_{t,\parallel}^2 \right\rangle} - \frac{\left\langle \mathbf{B}_0(\mathbf{x}) \cdot (\mathbf{e}_{\ell} \cdot \nabla)^2 \mathbf{B}_0(\mathbf{x}) \right\rangle}{B_{0,\parallel}^2 + \left\langle B_{t,\parallel}^2 \right\rangle} \ell^2 \quad (\text{A21})$$

still when $\ell \ll d$ and the displacement ℓ is limited to the plane-of-the-sky.

For our data sets we have the further simplification that $\delta < \ell \ll d$ and the dispersion function, equation (A21), has then a form similar to its three-dimensional counterpart with

$$\langle \Delta \Phi^2(\boldsymbol{\ell}) \rangle \simeq b^2 + m^2 \ell^2, \quad (\text{A22})$$

where

$$b^2 = \frac{2 \left\langle B_{t,\parallel}^2 \right\rangle}{B_{0,\parallel}^2 + \left\langle B_{t,\parallel}^2 \right\rangle} \quad (\text{A23})$$

is the quantity we evaluate through polarization measurements. Equation (A23) can be transformed to yield the ratio of the turbulent to large-scale magnetic field strength through

$$\frac{\langle B_{t,\parallel}^2 \rangle^{1/2}}{B_{0,\parallel}} = \frac{b}{\sqrt{2-b^2}}. \quad (\text{A24})$$

B. Data Analysis

Data from the Hertz polarimeter on the clouds studied here have been previously published by Houde et al. (2004) for OMC-1, Houde et al. (2002) for M17, and Kirby (2009) for DR21(Main). Details on the instrument as well as data acquisition and reduction can be found in Dowell et al. (1998) and Kirby et al. (2005), respectively. The analysis presented here is performed on a complete re-reduction of the raw Hertz data using the method of Kirby et al. (2005) and Dotson et al. (2009). The data may differ slightly from that published in the references above. For our purposes we only include data which satisfy the $P > 3\sigma_P$ criterion, where P is the polarization fraction and σ_P its uncertainty.

In each of the three objects the angle differences between each and every pair of data points are calculated as

$$\Delta\Phi_{ij} = \Phi_i - \Phi_j, \quad (\text{B1})$$

and the corresponding distance between each point

$$\ell_{ij} \equiv |\mathbf{x}_i - \mathbf{x}_j|. \quad (\text{B2})$$

Note that $\ell_{ij} = \ell_{ji}$ so that a map with N data points contains only $N(N-1)/2$ distinct differences. Also note that $|\Delta\Phi_{ij}|$ is constrained to be in the range $[0, 90]$ degrees.

These data are divided into separate distance bins with sizes corresponding to integer multiples of a single Hertz pixel-to-pixel separation ($17''.8$); the first bin covers $\ell_1 \leq \ell_{ij} < \ell_2$ (where ℓ_k corresponds to k pixels). Within each bin k we calculate the dispersion as the root-mean-square of the angle difference

$$\langle \Delta\Phi_{ij}^2 \rangle_k^{1/2} \quad \text{for all } \ell_k \leq \ell_{ij} < \ell_{k+1}. \quad (\text{B3})$$

The dispersion is corrected for measurement uncertainty within each bin according to equation (3). The uncertainty on each $\Delta\Phi_{ij}$ follows from simply propagating the measurement uncertainties on both Φ_i and Φ_j through equation (B1). The root-mean-square measurement uncertainties within each bin k are then given by

$$\sigma_{M,k} = \langle \sigma^2(\Delta\Phi_{ij}) \rangle_k^{1/2} \quad \text{for all } \ell_k \leq \ell_{ij} < \ell_{k+1}.$$

The corrected dispersions are those plotted for the different bins in Figure 2. The error bars in Figure 2 are determined by propagating the measurement uncertainties for Φ_i and Φ_j through equations (B1) and (B3), most of these are too small to be seen in the figure, especially at the smallest displacements.

For each object, the data are fitted to a linear model of the corrected square dispersion with respect to the square of the distance according to equation (2). In the discrete notation introduced in this section, the model is given by

$$\langle \Delta\Phi_{ij}^2 \rangle_k - \sigma_{M,k}^2 = b^2 + m^2 \ell_k^2.$$

In order to ensure we are in the linear regime, the fits are limited to only the smallest three distance bins. Taking into account the uncertainties on the $\langle \Delta\Phi_{ij}^2 \rangle_k$, the least-squares solutions for the parameter b are given in Table 1.

REFERENCES

- Chandrasekhar, S., and Fermi, E. 1953, *ApJ*, 118, 113
- Crutcher, R. M., Troland, T. H., Lazareff, B., Paubert, G., and Kazès, I. 1999, *ApJ*, L121
- Crutcher, R. M., Nutter, D. J., and Ward-Thompson 2004, *ApJ*, 600, 279
- Curran, R. L., and Chrysostomou, A. 2007, *MNRAS*, 382, 699
- Dotson, J. L., Davidson, J. A., Dowell, C. D., Hildebrand, R. H., Kirby, L., and Vaillancourt, J. E. 2009, submitted to *ApJS*
- Dowell, C. D., Hildebrand, R. H., Schleuning, D. A., Vaillancourt, J. E., Dotson, J. L., Novak, G., Renbarger, T., and Houde, M. 1998, *ApJ*, 504, 588
- Evans, N. J. II 1999, *ARA&A*, 37, 311
- Falceta-Gonçalves, D., Lazarian, A., and Kowal, G. 2008, *ApJ*, 679, 537
- Frisch, U. 1995, *Turbulence: The Legacy of A. N. Kolmogorov* (Cambridge: Cambridge University Press)
- Girart, J. M., Rao, R., and Marrone, D. P. 2006, *Science*, 313, 812

- Hoang, T., and Lazarian A. 2008, MNRAS, 388, 117
- Heitsch, F., Zweibel, E. G., Mac Low, M-M., Li, P., and Norman, M. L. 2001, ApJ, 561, 800
- Hiltner, W. A. 1949, ApJ, 114, 241
- Houde, M., Peng, R., Phillips, T. G., Bastien, P., and Yoshida, H. 2000, ApJ, 537, 245
- Houde, M., Bastien, P., Dotson, J. L., Dowell, C. D., Hildebrand, R. H., Peng, R., Phillips, T. G., Vaillancourt, J. E., and Yoshida, H. 2002, ApJ, 569, 803
- Houde, M. 2004, ApJ, 616, L111
- Houde, M., Dowell, C. D., Hildebrand, R. H., Dotson, J. L., Vaillancourt, J. E., Phillips, T. G., Peng, R., and Bastien, P. 2004, ApJ, 604, 717
- Kleiner S. C., and Dickman, R. L. 1984, ApJ, 286, 255
- Kleiner S. C., and Dickman, R. L. 1985, ApJ, 295, 466
- Kleiner S. C., and Dickman, R. L. 1987, ApJ, 312, 837
- Kirby 2009, ApJ, in press
- Kirby, L., Davidson, J. A., Dotson, J. L., Dowell, C. D., and Hildebrand, R. H. 2005, PASP, 117, 991
- Kudoh, T., and Basu, S. 2003, ApJ, 595, 842
- Lai, S.-P., Crutcher, R. M., Girart, J. M., and Rao, R. 2002, ApJ, 561, 864
- Lai, S.-P., Crutcher, R. M., Girart, J. M., and Rao, R. 2002, ApJ, 566, 925
- Lai, S.-P., Girart, J. M., and Crutcher, R. M. 2003, ApJ, 598, 392
- Lazarian, A., Vishniac, E. T., and Cho, J. 2004, ApJ, 603, 180
- Li, H., and Houde, M. 2008, ApJ, 677, 1151
- Myers, P. C., and Goodman, A. A. 1991, ApJ, 373, 509
- Ostriker, E. C., Stone, J. M., and Gammie, C. F. 2001, ApJ, 546, 980
- Padoan, P., Goodman, A. A., Draine, B. T., Juvela, M., Nordland, Å., and Rögnerdsson, Ö. E. 2001, ApJ, 559, 1005
- Schleuning, D. A. 1998, ApJ, 493, 811
- Vaillancourt, J. E. 2002, ApJS, 142, 53

Wiebe, D. S., and Watson, W. D. 2004, *ApJ*, 615, 314

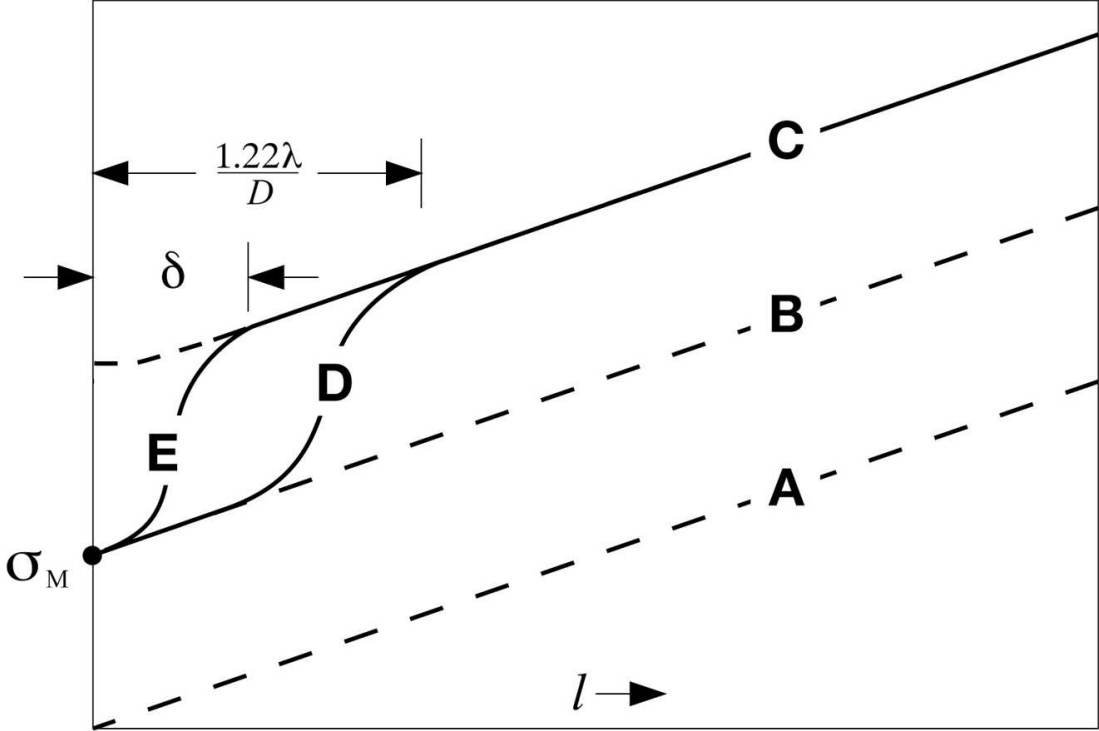


Fig. 1.— Dispersion: Idealized plots of the angular dispersion function, $\langle \Delta \Phi^2(\ell) \rangle^{1/2}$, between pairs of magnetic field vectors separated by displacements ℓ , for values of $\ell \ll d$, with d the typical length scale for variations in the large-scale magnetic field (see §3). Curve A: no measurement uncertainty; no turbulence. Curve B: with measurement uncertainty, σ_M . Curve C: with turbulence. Curves D and E: accounting for correlation in polarization angles at displacements ℓ smaller than the larger of the telescope beam ($1.22\lambda/D$) (Curve D) or the turbulent correlation length δ (Curve E).

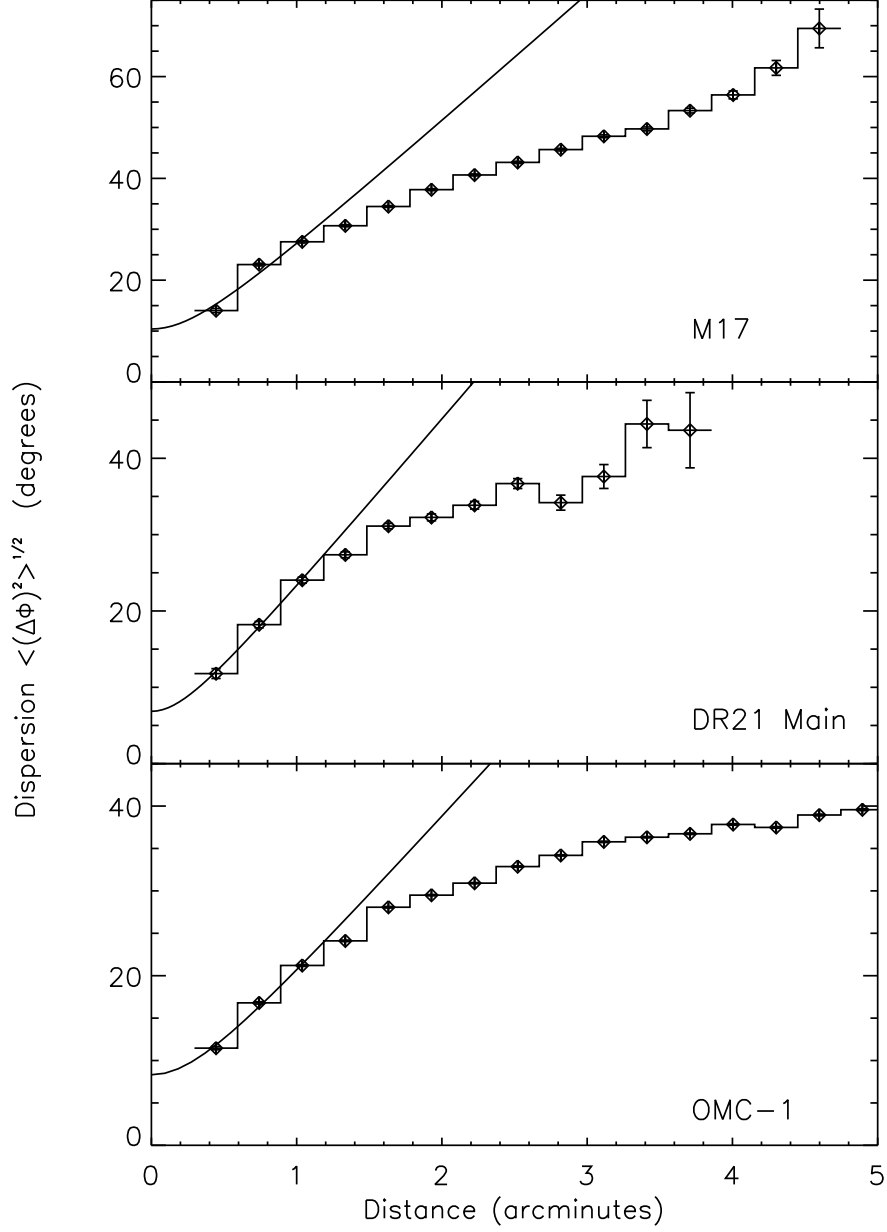


Fig. 2.— Angular dispersion function, $\langle\Delta\Phi^2(\ell)\rangle^{1/2}$, for M17, DR21(Main), and OMC-1. The turbulent contribution to the total angular dispersion is determined by the zero intercept of the fit to the data at $\ell = 0$. The measurement uncertainties were removed prior to operating the fits to the corresponding data sets. The results are given in Table 1.

Table 1. Results for the dispersion, the turbulent to mean magnetic field strength ratio, the line widths, and the mean field strength.

Object	b^a (deg)	$\langle B_t^2 \rangle^{1/2} / B_0^b$	$\sigma(v)$ (km s ⁻¹)	B_0^c (mG)
OMC-1	8.3 ± 0.3	0.10 ± 0.01	1.85	3.8
M17	10.4 ± 0.6	0.13 ± 0.01	1.66	2.9
DR21(Main)	6.8 ± 1.3	0.08 ± 0.02	4.09	10.6

^aTurbulent dispersion (i.e., the dispersion limit as $\ell \rightarrow 0$).

^bCalculated with equation (7).

^cCalculated with equation (8), assumes a density of 10^5 cm⁻³ and a mean molecular weight of 2.3. These estimates are not precise to better than a factor of a few. The process of signal integration through the thickness of the cloud and across the telescope beam inherent to the polarization measurements has also not been taken into account.